Proceedings of the Korean Nuclear Society Spring Meeting
Kwangju, Korea, May 1997

An Investigation of Thermal Margin for External Reactor Vessel Cooling (ERVC) in Large Advanced Light Water Reactors (ALWR)

Jong Woon Park and Dong Wook Jerng
Korea Electric Power Research Institute
Korea Electric Power Corporation
103-16, Munji-dong, Yusung-gu
Taejon, Korea 305-380

Abstract

A severe accident management strategy, in-vessel retention of corium through external reactor vessel cooling (ERVC) is being studied worldwide as a means to prevent reactor vessel failure following a core melt accident. An evaluation of feasibility of this ERVC for a large Advanced Light Water Reactor (ALWR) is presented. To account for the coolability of corium and metal in the reactor vessel, a thermal analysis is performed using an existing method. Results show that the peak heat flux along the inner surface of the reactor vessel lower head has a relatively smaller margin than a small capacity reactor such as AP600 in regards with the critical heat flux attainable at the outer surface of the reactor vessel lower head.

1. Introduction

A primary feature of advanced light water reactor (ALWR) is its design consideration for the prevention and the mitigation of consequences of core melt in severe accident conditions. The in-vessel retention (IVR) concept (i.e., external reactor vessel cooling: ERVC), one of the severe accident management strategies, provides the cooling of the corium by removing decay heat through the water flooded in the reactor cavity before corium relocates to the reactor pressure vessel (RPV) lower plenum. In this strategy, the heat transfer regime on the external surface should be maintained as nucleate boiling in order to effectively remove the decay heat without boiling crisis. A measure of whether this strategy could succeed is a thermal margin defined as a ratio of critical heat flux to the actual heat flux on the reactor vessel external surface.

The corium coolability by ERVC has been analytically and experimentally evaluated by Theofanous et al.[1] for AP600 and by Kymäläinen for Loviisa (VVER-440) [2]. The primary reason that these plants can accommodate IVR is a small power with large RCS water volume. In case of a large ALWR(~1300 MWe), it could be qualitatively stated that the thermal margin will be smaller since, compared to AP600 like reactors, it has a larger power density which may lead to a faster accident progression, and a smaller in-vessel steel mass inventory which will result in a higher focusing effect due to metallic layer[1]. Table 1 summarizes the relevant plant features and parameters of a typical large ALWR compared to AP600 in relation to the analysis of the IVR feasibility.

Although the thermal margin of a large ALWR would be intuitively expected to be low, the margin for a large ALWR has never been quantitatively assessed yet, and thus, if it is quantified by appropriate and reasonable methodology we can obtain insights into the applicability of the IVR to the large ALWRs. In this paper, therefore, applicability of the ERVC for the large ALWR is preliminarily assessed by quantifying the thermal margin, that is, a thermal load analysis is performed by using a methodology developed by Theofanous [1] for the modeling of heat transfer between oxide pool, metallic layer, lower head and side wall [1] to evaluate the magnitude of heat flux imposed on the reactor vessel wall.

2. Thermal Load Analysis

A physical model [1] is illustrated in Fig. 1 depicting the condition in which most of the molten core oxide material, namely UO_2 and ZrO_2, relocated to the reactor vessel lower plenum forming a molten pool, and molten metallic layer relocated as a separate phase on the top of the pool. The decay heat $\dot{Q}$ in the oxide pool is partitioned into upward and downward heat flow driven by natural convection phenomenon in the inside of the oxide pool. The respective heat fluxses are denoted as q''_{up} and q''_{dn} in Fig. 1. The heat transferred upwards from the oxide pool goes to the metallic layer, which is also divided into the heat convected to the upper film of the metallic layer and the heat conducting to the side wall of the reactor vessel of which flux is designated as q''_{lw} in Fig 1. The heat convected to the upper film of the metallic layer is finally radiated from the upper boundary surface.

Melt Pool Heat Transfer

For the analytical formulation of the heat transfer mechanism inside the oxide pool, The major assumptions involved are as follows [1]: (1) The oxide pool contains the oxidic components of the core melt (mainly UO_2 and ZrO_2), with a liquidus of about 2973 K. This very high temperature liquidus enclosed by the cooling wall makes this pool completely surrounded by crusts; (2) The crust is thin enough not to appreciably alter the shape of the enclosure, and they impose a uniform temperature boundary condition - the melt liquidus. As a consequence, the pool-internal heat transfer problem is decoupled from outside as long as the crust remains between the reactor vessel wall and oxide pool.

The overall energy balance for the oxide melt pool is thus obtained simply by equating the heat generated inside the oxide pool to the sum of up- and downward heat flows [1] (the meaning of the variables in the following formulation is indicated in Fig. 1):

$$V\dot{Q} = s_{up}q''_{up} + s_{dn}q''_{dn} \tag{1}$$

$$q''_{dn} = \frac{V\dot{Q}}{s_{dn}\left(1+\frac{s_{up}}{s_{dn}}R'\right)} \tag{2}$$

where V is the volume of the melt, $\dot{Q}$ is the decay heat generation per unit volume of melt, s_{up} and s_{dn} are the flat and curved areas respecively of the surfaces of the hemispherical segment, q''_{up} and q''_{dn} are the average up- and down-ward heat fluxes, respectively. The upward heat flux q''_{up} can be obtained from:

$$q''_{up} = h_{up}(T_{max} - T_m) \tag{3}$$

where h_{up} is the heat transfer coefficients obtained from a Nusselt number which will be defined later in this section. R' in Eq.(2) is defined to be the ratio of the up-to-down heat fluxes obtained from:

$$R' = \frac{q''_{up}}{q''_{dn}} = \frac{Nu_{up}}{Nu_{dn}} \tag{4}$$

The Nusselt numbers in Eq.(4) for the oxide melt pool natural convection are given by following:

$$Nu_{up} = 0.345Ra'^{0.233} \text{ (Steinberner and Reineke [3])} \tag{5}$$

for the upward natural convection, and

$$Nu_{dn} = 0.0038Ra'^{0.35} \text{ (Theofanous et al. [1]), or} \tag{6a}$$

$$Nu_{dn} = 0.55Ra'^{0.2} \text{ (Mayinger et al. [4])} \tag{6b}$$

for the downward convection. And the Rayleigh numbers Ra' in Eqs.(5) and (6) are defined by

$$Ra' = \frac{g\beta H^5 Q}{\alpha\nu k} \tag{7}$$

Metallic Layer Focusing Effect

For the energy balance of the metallic layer, following simplifying assumptions have been applied: (1) The metallic layer has a large aspect ratio (thin compared to the diameter) and is almost vertical to the

side wall, i.e., reactor vessel wall, and the side boundary temperature is fixed - at the liquidus of metallic layer of ~1300 °C; (2) the properties at the upper, lower and side boundaries are all the same; (3) the upper and lower boundaries of the metallic layer have the same area; (4) the crust between the oxidic pool and metallic layer is thin (5) the energy radiated from the reactor vessel inner surface to the metallic layer is negligible.

Based on the above assumptions, and since the heat transferred upward from the oxide pool divides into the heat convected to the upper film and the heat to the side wall, overall energy balance in the metallic layer can be obtained and rearranged as follows [1]:

$$q_{up}^{"} = (\varepsilon\sigma)T_{l,o}^4 + A\left(\frac{H_l}{R}\right)\left[(T_{l,o} - T_{l,m}) + \left(\frac{\varepsilon\sigma}{A}\right)^{3/4} T_{l,o}^3\right]^{4/3} \quad (8)$$

where ε is the emissivity of the metallic layer top surface and A is the thermo-physical parameter given by

$$A = 0.15k\left(\frac{g\beta}{\alpha\nu}\right)^{1/3} \quad (9)$$

And the energy balance where the heat convected to the upper film is equal to the heat radiated from the upper boundary surface gives [1]:

$$T_b = T_{l,o} + \left(\frac{\varepsilon\sigma}{A}\right)^{3/4} T_{l,o}^3 \quad (10)$$

Equation (8), firstly, can be solved by using bisection method to obtain $T_{l,o}$ given q_{up} calculated from the melt pool heat transfer model, i.e., Eqs.(3) and (5), secondly Eq.(10) is used for T_b, and finally T_{max} is calculated from following equation which can be derived from Eq.(1):

$$\Delta T_m = T_{\max} - T_m = \frac{V\dot{Q}}{\frac{k}{H}(s_{dn}q_{dn}^{"} + s_{up}q_{up}^{"})} \quad (11)$$

After T_b is known, the heat flux to the side wall can be obtained from:

$$q_{lw}^{"} = A(T_b - T_{l,m})^{4/3} \quad (12)$$

Plant specific parameters and thermo-physical properties used in this calculation are shown in Table 2.

Heat Flux distribution as a function of the Angular Position

The downward heat flux obtained from Eq.(2) is an average value. The local downward heat flux along the surface of the lower head can be obtained from the heat flux distribution as a function of the angular position [1]:

$$\frac{q_{dn}^{"}(\theta)}{q_{dn}^{"}} = \frac{Nu_{dn}(\theta)}{Nu_{dn}} = 0.1 + 1.08\left(\frac{\theta}{\theta_p}\right) - 4.5\left(\frac{\theta}{\theta_p}\right)^2 + 8.6\left(\frac{\theta}{\theta_p}\right)^3, \quad 0.1 \le \frac{\theta}{\theta_p} \le 0.6 \quad (13a)$$

$$\frac{q_{dn}^{"}(\theta)}{q_{dn}^{"}} = \frac{Nu_{dn}(\theta)}{Nu_{dn}} = 0.41 + 0.35\left(\frac{\theta}{\theta_p}\right) + \left(\frac{\theta}{\theta_p}\right)^2, \quad 0.6 \le \frac{\theta}{\theta_p} \le 1 \quad (13b)$$

According to Eq.(13), the peak value appears at the position with highest angle ($\theta/\theta_p = 1$), i.e., at the top edge of the lower boundary of the melt pool.

Critical Heat Flux at the Outer Surface of the Lower Head

Heat removal capability at the outer surface of the reactor vessel lower head is limited by the critical heat flux. The existing critical heat flux correlations directly applicable to the reactor condition are those developed from the ULPU-2000 Configuration II experiment [5] and it is given by

$$q_{cr}^{"}(\theta) = 500 + 13.3\theta \quad \text{kW/m}^2, \quad q < 15^\circ \quad (14a)$$

$$q_{cr}^{"}(\theta) = 540 + 10.7\theta \quad \text{kW/m}^2, \quad 15^\circ < q < 90^\circ \quad (14b)$$

If either the local downward or the sideward heat flux is greater than the critical heat flux from Eq.(13), the coolant condition at the outer surface of the lower head transits from nucleate boiling to film boiling regime. In this condition, the heat generation rate is greater than the removal rate so the temperature of the lower head will continuously rise and consequently fail. In order for the integrity of lower head to be maintained, therefore, at least the peak downward heat flux from the melt pool to the lower head should be less than the critical heat flux.

3. Results and Conclusion

The average and peak heat flux estimated by the aforementioned formulation to the lower head and side wall in the large ALWR lower head are shown in Table 4 in comparison with the results of AP600. The plant specific parameters and thermo-physical properties used in this thermal load analysis are shown in Table 2. The value of melt mass and the decay heat are extracted from MAAP4 [6] simulation results at 2.42 hr (just before the RPV failure occurs) for the sequence of large LOCA (0.5 ft^2) with safety injection failure.

High thermal power and power density of the large ALWR result in lower thermal margin for cooling of lower head and side wall of the reactor vessel. When the downward Nusselt number correlation of Eq.(6a) is applied to the formulation of the oxide pool, the average heat flux to the lower head is calculated to be 650 kW/m^2, and, when Eq.(6b) is applied, it is 501 kW/m^2. Since the angle θ_p is 85°, the peak heat flux locates in this angle and is calculated by applying Eq.(13b) to be 1143 kW/m^2 and 882 kW/m^2 based in Eqs.(6a) and (6b), respectively. And the critical heat flux at θ=85° is calculated from Eq.(13b) to be 1452 kW/m^2, and therefore the thermal margins are 27% and 64% depending on which correlation is used, i.e., Eqs.(6a) and (6b).

The heat fluxes to the sidewall from metallic layer calculated for each correlation of Eq.(6a) and (6b) are 880 $kW/m^2$and 1269 kW/m^2. The magnitude of this sideward heat flux is larger for the smaller value of downward heat flux of the oxide pool since upward heat flux, which contributes as heat source of the metallic layer, increases as downward heat flux decreases. Therefore, it can be noted that sideward heat flux increases as downward heat flux decreases, and vice versa. The direction of sideward heat flux is nearly 90° from the centerline, and therefore critical heat flux at the outer surface obtained with this angle from Eq.(13b) is 1503 kW/m^2. The margins are 71% and 18% depending also on the correlations.

In this paper, a calculation was performed to obtain an insight to the applicability of the IVR concept to a large power reactor. As expected, the thermal margin which is a measure of applicability was found to be considerably small. Although a reactor with a 4000 MWt capacity may have a thermal margin from the heat removal point of view, the margin may be so small that the uncertainties involved in the applied model may sweep it out. Therefore, a careful and precise investigation is essential to take the IVR concept for a large capacity reactor, because the thermal load is strongly dependent on the core melt progression phenomena which comprise a wide spectrum of uncertainty yet. Also there are rooms to improve the analytic model to include the radiative heat transfer between metallic layer and the upper internal structures and radial heat conduction through metallic layer due to the temperature distribution along radial direction. However, benefit obtained from considering such effect will not overcome the complexity of the modeling and uncertainty of such major input parameters as oxide pool height, steel mass, height of the metallic layer, shutdown time, decay power density, thermo-physical properties, so on.

References

1. T.G. Theofanous, C. Lui, S. Additon, S. Angelini, O. Kym l inen, T. Salmassi, *In-Vessel Coolability and Retention of a Core Melt,* DOE/ID-10460.
2. O. Kymäläinen, "Loviisa 1 & 2, In-Vessel Retention of Corium During a Severe Accident", IVO International, Ltd. Report L01-GT1-64.
3. U. Steinberner and H.H. Reineke, Turbulent Buoyancy Convection Heat Transfer with Internal Heat Sources, Proc. Sixth Int. Heat Transfer Conference, Toronto, Canada, August, 1978.

4. F. Mayinger, M. Jahn, H. Reineke, and U. Streiberner, "Examination of Thermohydraulic Processes and Heat Transfer in a Core Melt", Final Report BMFT RS 48/1. Thechnical University, Hannover, W. Germany, 1975.
5. T.G. Theofanous et al., "Critical Heat Flux through Curved, Downward Facing Thick Walls", *Nuclear Engineering and Design*, Vol. 151, pp.247-258, 1994.
6. R.E. Henry, C.Y. Paik, and M.G. Plys, "MAAP 4 - Modular Accident Analysis Program for LWR Power Plants", Vol. 1-4, Fauske & Associates, Inc., 1994.

Table 1. Plant parameters of interest to IVR between AP600 and the large ALWR

Plant Parameters	AP600	The Large ALWR
Thermal Power	1933 MWt	4000 MWt
Power Density	73 kW/l	98.4 kW/l
In-Vessel Steel Mass [a]	107 ton	88.7 ton
Upper Internal	46.5 ton	77.2 ton
Core Region	80 ton	59.2 ton
Lower Internal	27 ton	29.5 ton
Cable Location	Upper Head Region	Lower Head Bottom
Water Volume to Fill Cavity [b]	122 m^3	845 m^3
RCS Free Volume	137 m^3	396 m^3
ECCS Inventory	209.3 m^3 (2 CMT+2 ACC)	217.6 m^3(4 SITs)
ECCS Inventory /RCS Vol.	1.53	0.55

[a] Reflector, Core Barrel, Lower Internals; [b] Upto the Bottom of The Active Fuel

Table 2. Plant specific parameters and thermo-physical properties used

Plant Specific Parameters	AP600		The Large ALWR	
Lower Head Avg. Radius (R_{LH})	2 m		2.05 m[b]	
Angle of Filling LP (f)	74° (100 % Melt) [a]		85° (83% Melt)	
Decay Heat (Q)	13 MW (7.5 hr) [a]		26 MW (2.4 hr) [c]	
Melt Volume (V)	10.0 m^3 [a]		15.7 m^3 [c]	
Decay Heat per Unit Volume ($\dot{Q}$)	1.30 MW/m^3		1.65 MW/m^3	
Metallic Layer Thickness (H_l)	0.4 x R_{LH} (64% TI[d])		0.327 x R_{LH} (100% TI)	
Thermo-physical Properties	Oxide Pool [e]	Metallic layer [f]	Oxide Pool	Metallic layer
Melting Temperature	2973	1600	2973	1600
Density (ρ, kg/m^3)	8450	6890	8450	6890
Conductivity (k, $W/m\text{-}K$)	5.3	25.5	5.3	25.5
Specific Heat (c_p, $W/kg\text{-}K$)	510	778	510	778
Viscosity (μ, Pa-s)	5.3×10^{-3}	4.2×10^{-3}	5.3×10^{-3}	4.2×10^{-3}
Linear Expansion Coefficient (K^{-1})	1.05×10^{-4}	1.1×10^{-4}	1.05×10^{-4}	1.1×10^{-4}
Thermal Diffusivity (α, m^2/sec)	1.23×10^{-6}	4.76×10^{-6}	1.23×10^{-6}	4.76×10^{-6}
Emissivity	N/A	0.45	N/A	0.45
Rayleigh Number (Ra')	2.1×10^{15}	N/A	9.6×10^{15}	N/A
Property Group A for Metallic layer [g]	N/A	2764	N/A	2751

[a] Data from DOE/ID-10460 [1]; [b] Horizontal Radius = 2.31 m; Vertical Height = 1.7 m;
[c] Data from MAAP4 output for LL-3 sequence at 2.42 hr just before the lower head failure occurs;
[d] T I = Total Inventory (Side and Lower Part of Core); reflector included for AP600
[e] 90% UO_2 and 10% ZrO_2; [f] 90% Fe and 10% Zr; [g] Eq.(9)

Table 3. Oxide Melt Pool Heat Fluxes and Metallic Layer Focusing Effect Analysis Result

Values	AP600	The Large ALWR
Pool Superheat (ΔT_m, K)	116 (134)	154 (206)
Avg. Downward Heat Flux (q_{dn}, kW/m^2)	370 (312)	650 (501)
Max. Downward Heat Flux ($q_{dn,max}$, kW/m^2)	653 (550)	1143 (882)
CHF at the Top edge of Pool (q_{CHF}, kW/m^2)	1332	1452
Thermal Margin ($q_{CHF}/q_{dn,max}$ -1)	104%(142%)	27%(64%)
Upward Heat Flux (q_{up}, kW/m^2)	538 (630)	788 (1063)
Sideward Heat Flux through Metallic layer (q_{lw}, kW/m^2)	436 (543)	880 (1269)
CHF at the Side Wall (q_{CHF}, kW/m^2)	1503	1503
Thermal Margin (q_{CHF}/q_{lw} -1)	245%(177%)	71%(18%)

(Note) Eq.(6a) and Eq.(6b) are used for the values out of the bracket and inside the bracket, respectively

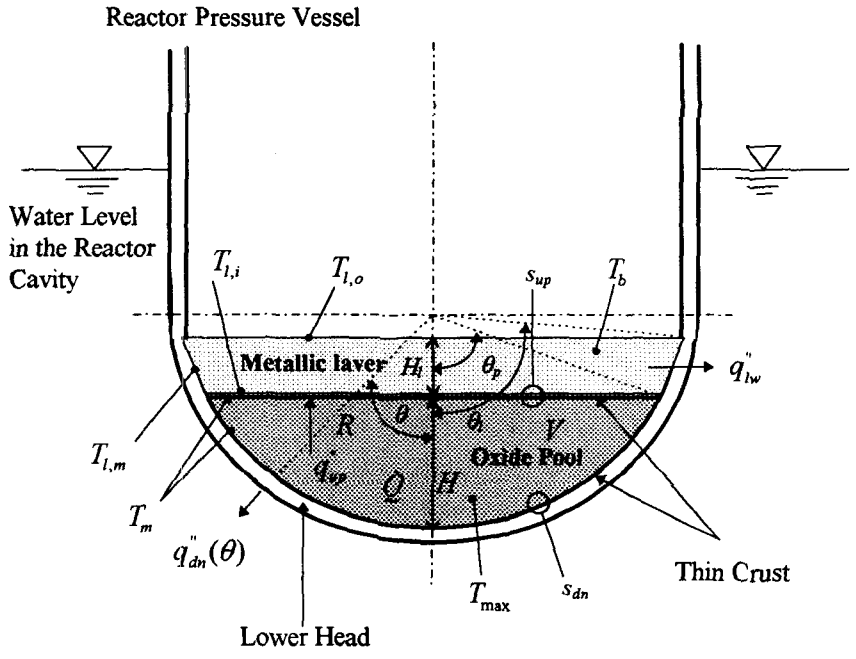

Fig. 1 Physical model for the thermal load analysis. Also shown is the nomenclature used in the formulation of the mathematical model [1]